IOPscience iopscience.iop.org

Home Search Collections Journals About Contact us My IOPscience

A spectral model of stably stratified surface-layer turbulence

This content has been downloaded from IOPscience. Please scroll down to see the full text.

2015 J. Phys.: Conf. Ser. 625 012003

(http://iopscience.iop.org/1742-6596/625/1/012003)

View the table of contents for this issue, or go to the journal homepage for more

Download details:

IP Address: 130.238.171.215
This content was downloaded on 31/08/2015 at 12:21

Please note that terms and conditions apply.

A spectral model of stably stratified surface-layer turbulence

A. Segalini[1], J. Arnqvist[2], I. Carlén[3], H. Bergström[2] & P. H. Alfredsson[1]

[1] Linné FLOW Centre, KTH Mechanics, Osquars Backe 18, 10044 Stockholm
[2] Dept. Earth Sc., Uppsala University, Villavagen 16, 75236 Uppsala
[3] TG Teknikgruppen AB, Kemistvägen 6, 18379 Täby

E-mail: segalini@mech.kth.se

Abstract. A new model to determine the spectral velocity tensor in a stably stratified flow is proposed. This model is complementary to the Mann model as it solves the stratified inviscid Rapid Distortion Theory equations analytically, allowing for the determination of the single and two-point velocity spectra as well as the temperature-velocity cross-spectra. The model has been here calibrated and validated against field measurements conducted over a forested area with measurements up to 140 m, therefore covering a region of interest for wind-energy applications.

1. Introduction

The knowledge of the instantaneous velocity field characteristics of the atmospheric boundary layer has crucial importance for an efficient wind-energy utilisation. However, the flow over the rotor is highly turbulent and depends on a large number of parameters, like the boundary-layer height, the geostrophic-wind variation and the surface inhomogeneities, to mention some. Wind turbines must be designed to operate in and withstand such a turbulent environment. The current physical understanding of turbulent motions comes from experiments (in real fields or wind tunnels) and numerical simulations. In the latter case the high Reynolds number of the flow becomes challenging because of the increasing scale separation between large and small eddies both inside the domain and at the upstream domain boundaries. In order to obtain a realistic turbulent velocity field, we must force a realistic turbulent field at the inlet of the computational domain with prescribed characteristics or, alternatively, use a precursor simulation that serves as input for the main simulation. The latter approach provides a realistic field but it has the cost of additional computational power that is needed to provide the input for the main simulation. The former method, on the other hand, is quite efficient but necessitates of some information about the boundary-layer velocity field and its temporal characteristics. The model developed by Mann [1], for instance, provides a description of the spectral velocity tensor (Φ_{ij}, where i and j correspond to the fluctuating velocity components u', v' and w', indicating the streamwise, lateral and vertical velocity components, respectively) that can be used to determine the single- and two-point spectra of velocity time series inside and at the boundaries of the numerical domain. This approach provides some information about the frequency distribution of the energy so that a synthetic velocity field can be created that has the same one- and two-point

Content from this work may be used under the terms of the Creative Commons Attribution 3.0 licence. Any further distribution of this work must maintain attribution to the author(s) and the title of the work, journal citation and DOI.
Published under licence by IOP Publishing Ltd

statistics of the observed one. Since 1994, the model has become the standard tool to synthesise turbulence time series at the inlet of many numerical simulations aimed at the characterisation of unsteady loads and aeroelastic effects.

However, the Mann model provides results in absence of density stratification and empirical approaches must be used to extend its application to non-neutral conditions (see for instance [2]). The absence of a density equation in the Mann model limits its use as an in-flow tool since, in addition to the initial velocity spectrum, models with non-neutral stratification need a description of the initial temperature spectrum.

The Mann model is based on Rapid Distortion Theory (RDT) where the turbulence is driven by the mean-flow distortion rather than by the non-linear distortions by turbulence itself. As the theory is time-dependent, a characteristic time scale is introduced to stop the structures evolution at a time related to their expected lifetime. In order to extend the model to stratified conditions, a solution of the inviscid stratified RDT equations with homogeneous shear is proposed, extending the solution of Hanazaki and Hunt [3] to the two horizontal velocity components. The analytical solution allows for the determination of the spectra at any given time, starting from a prescribed initial condition. Following the same approach adopted by Mann [1], a model for the spectral velocity tensor in the atmospheric surface layer is obtained where the spectral tensor, assumed to be isotropic at the initial time, evolves until the break-up time, where the spectral tensor is supposed to achieve its equilibrium state observed in surface-layer turbulence. A similar approach was developed by Chougule [4] by numerically integrating the stratified RDT equations.

The present paper aims at assessing whether or not the new extended model (discussed in section 2) can be used to simulate realistic atmospheric turbulence (as the Mann model does) with the additional information that regards the heat fluxes and, in general, the temperature-velocity correlations for different stability classes. Here only stably stratified conditions will be discussed, although the model can be extended to unstable stratification as well. Data from a measurement campaign over a forested site (section 3) will be used to calibrate and validate the model (section 4). Section 5 will conclude the paper with some final remarks.

2. Mathematical model

Let us consider a homogeneously stratified flow (with constant $\mathrm{d}\rho_0/\mathrm{d}z$) with a uniform mean velocity shear in the z-direction. By normalising physical variables with the characteristic length and velocity scale L and U_s (for the moment left unspecified), the dimensionless inviscid RDT governing equations can be written in Fourier space (where the $\hat{\cdot}$ indicates the Fourier transform operator) as

$$\frac{\mathrm{d}\hat{u}}{\mathrm{d}t} = \alpha\left(\frac{2k_x^2}{k^2} - 1\right)\hat{w} + \frac{k_x k_z}{k^2}\hat{\rho}\,, \tag{1}$$

$$\frac{\mathrm{d}\hat{v}}{\mathrm{d}t} = \alpha\frac{2k_x k_y}{k^2}\hat{w} + \frac{k_y k_z}{k^2}\hat{\rho}\,, \tag{2}$$

$$\frac{\mathrm{d}\hat{w}}{\mathrm{d}t} = \alpha\frac{2k_x k_z}{k^2}\hat{w} + \left(\frac{k_z^2}{k^2} - 1\right)\hat{\rho}\,, \tag{3}$$

$$\frac{\mathrm{d}\hat{\rho}}{\mathrm{d}t} = N^2\hat{w}\,, \tag{4}$$

where $\alpha = \mathrm{d}U/\mathrm{d}z L/U_s$ is the dimensionless mean wind shear, $N = \left[-\left(g/\rho_0\right)\left(\mathrm{d}\rho_0/\mathrm{d}z\right)\right]^{1/2} L/U_s$ is the scaled Brunt-Väisälä frequency, g is the gravitional acceleration, $k = \left(k_x^2 + k_y^2 + k_z^2\right)^{1/2}$ is the wavenumber magnitude and the density is normalised as $\rho/(\rho_0 \mathrm{Fr}^2)$ where $\mathrm{Fr} = U_s/\left(gL\right)^{1/2}$ is the characteristic Froude number.

The equation for the evolution of the wavenumber vector, $\mathbf{k}(t) = (k_x,\, k_y,\, k_z)$, is [5]

$$\frac{\mathrm{d}k_x}{\mathrm{d}t} = \frac{\mathrm{d}k_y}{\mathrm{d}t} = 0 \quad , \quad \frac{\mathrm{d}k_z}{\mathrm{d}t} + \alpha k_x = 0 \quad \longrightarrow \quad \mathbf{k} = (k_{x0},\, k_{y0},\, k_{z0} - \alpha k_{x0} t) \;, \tag{5}$$

where $(k_{x,0},\, k_{y,0},\, k_{z,0})$ is the initial wavenumber vector with magnitude k_0. As a notation, the horizontal wavenumber $k_h = \left(k_x^2 + k_y^2\right)^{1/2}$ is introduced, a quantity that, according to equation (5), is independent of time.

As discussed in the introduction, Hanazaki & Hunt [3] provided an analytical solution of the stratified RDT equations for equations (3) and (4). The solution is based on the introduction of the variable $\zeta = ik_z/k_h$ in the equation which results from the combination of the density and vertical-velocity equations, leading to the differential equation

$$\left(1 - \zeta^2\right) \frac{\mathrm{d}^2\hat{\rho}}{\mathrm{d}\zeta^2} - 2\zeta \frac{\mathrm{d}\hat{\rho}}{\mathrm{d}\zeta} + \lambda\left(1 + \lambda\right)\hat{\rho} = 0 \,, \tag{6}$$

where

$$\lambda\left(1 + \lambda\right) = -\frac{N^2 k_h^2}{\alpha^2 k_x^2} \,. \tag{7}$$

Equation (6) can be solved in terms of Legendre functions of first and second order as

$$\hat{\rho} = A P_\lambda\left(\zeta\right) + B Q_\lambda\left(\zeta\right) \;, \tag{8}$$

while the vertical-velocity Fourier transform is

$$\hat{w} = -\frac{i\alpha k_x}{N^2 k_h} \left[A P'_\lambda\left(\zeta\right) + B Q'_\lambda\left(\zeta\right)\right] \;, \tag{9}$$

in which the primes indicate the derivative of the Legendre functions with respect to their argument ζ.

After some algebra [6], it is possible to get the analytical solution for the other two velocity components as

$$\hat{u} = \hat{u}_0 + \frac{\alpha}{N^2 k_h^2} \left\{ A \left[k_x^2\, \zeta P'_\lambda\left(\zeta\right) - k_y^2\, P_\lambda\left(\zeta\right)\right]_{\zeta_0}^{\zeta} + B \left[k_x^2\, \zeta Q'_\lambda\left(\zeta\right) - k_y^2\, Q_\lambda\left(\zeta\right)\right]_{\zeta_0}^{\zeta} \right\} , \tag{10}$$

$$\hat{v} = \hat{v}_0 + \frac{\alpha k_x k_y}{N^2 k_h^2} \left\{ A \left[\zeta P'_\lambda\left(\zeta\right) + P_\lambda\left(\zeta\right)\right]_{\zeta_0}^{\zeta} + B \left[\zeta Q'_\lambda\left(\zeta\right) + Q_\lambda\left(\zeta\right)\right]_{\zeta_0}^{\zeta} \right\} , \tag{11}$$

where $\zeta_0 = ik_{z,0}/k_h$ indicates the value of ζ at the initial time.

The constants A and B can be determined through the initial-density and vertical-velocity fluctuations Fourier transforms by solving the linear system

$$\begin{bmatrix} P_\lambda\left(\zeta_0\right) & Q_\lambda\left(\zeta_0\right) \\ P'_\lambda\left(\zeta_0\right) & Q'_\lambda\left(\zeta_0\right) \end{bmatrix} \begin{bmatrix} A \\ B \end{bmatrix} = \begin{bmatrix} \hat{\rho}_0 \\ \left(iN^2 k_h \hat{w}_0\right) / \left(\alpha k_x\right) \end{bmatrix} . \tag{12}$$

The time evolution of the velocity and density perturbation vector $\mathbf{q} = [\hat{u},\, \hat{v},\, \hat{w},\, \hat{\rho}]^T$ from its initial state $\mathbf{q}_0 = [\hat{u}_0,\, \hat{v}_0,\, \hat{w}_0,\, \hat{\rho}_0]^T$ can be written as $\mathbf{q} = \mathbf{M}\mathbf{q}_0$ where the matrix $\mathbf{M}$ is given by

$$\mathbf{M}\left(t; \mathbf{k}_0\right) = \begin{bmatrix} 1 & 0 & F_{uw_0} & F_{u\rho_0} \\ 0 & 1 & F_{vw_0} & F_{v\rho_0} \\ 0 & 0 & F_{ww_0} & F_{w\rho_0} \\ 0 & 0 & F_{\rho w_0} & F_{\rho\rho_0} \end{bmatrix} , \tag{13}$$

with the coefficients obtained from equations (10), (11), (9) and (8) and reported in [6].

The generic time-dependent spectral matrix $\mathbf{\Phi}(t;\mathbf{k})$ is now introduced as

$$\mathbf{\Phi}(t;\mathbf{k}) = \Re\left[\overline{\mathbf{q}(t)\mathbf{q}^{T*}(t)}\right] = \begin{bmatrix} \Phi_{xx} & \Phi_{xy} & \Phi_{xz} & \Phi_{x\rho} \\ \Phi_{xy} & \Phi_{yy} & \Phi_{yz} & \Phi_{y\rho} \\ \Phi_{xz} & \Phi_{yz} & \Phi_{zz} & \Phi_{z\rho} \\ \Phi_{x\rho} & \Phi_{y\rho} & \Phi_{z\rho} & \Phi_{\rho\rho} \end{bmatrix}, \tag{14}$$

where the $*$ superscript indicates the complex conjugate operator. The evolution of the spectral tensor (14) is given by

$$\mathbf{\Phi}(t;\mathbf{k}) = \mathbf{M}(t;\mathbf{k}_0)\,\mathbf{\Phi}(0;\mathbf{k}_0)\,\mathbf{M}^T(t;\mathbf{k}_0)\,. \tag{15}$$

Equation (15) is the key result of this work since it determines the evolution of the spectral tensor of velocity and density fluctuations starting from a generic initial condition $\mathbf{\Phi}(0;\mathbf{k}_0)$ after a generic time t.

The dimensionless initial velocity field can be assumed to be isotropic and characterised by means of the von-Kármán spectrum [1] that, according to the present scaling, becomes

$$\Phi_{ij}(0;\mathbf{k}_0) = \frac{Q_u}{4\pi}\,\frac{\delta_{ij}k_0^2 - k_{i,0}k_{j,0}}{\left(1+k_0^2\right)^{17/6}} \qquad \text{with} \qquad Q_u = \frac{\alpha_1\epsilon^{2/3}L^{2/3}}{{U_s}^2}\,, \tag{16}$$

where ϵ is the turbulent kinetic energy dissipation rate and α_1 is the Kolmogorov constant [7]. The corresponding isotropic dimensionless density spectrum can be also written as a power law [8] as

$$\Phi_{\rho\rho}(0;\mathbf{k}_0) = \frac{Q_\rho}{\left(1+k_0^2\right)^{11/6}} \qquad \text{with} \qquad Q_\rho = \frac{5\beta_1}{6\pi\alpha_1}\,\frac{1}{\mathrm{Fr}^4}\,\frac{\epsilon_\rho {U_s}^2}{{\rho_0}^2\epsilon}Q_u\,, \tag{17}$$

where ϵ_ρ is the dissipation rate of half the density variance and β_1 is a universal constant [7]. Equations (16) and (17) characterise the initial spectral tensor and allow some flexibility by means of the parameters Q_u and Q_ρ that represent two important properties of the initial isotropic field: Q_u is the normalised turbulent kinetic energy dissipation of the velocity field, while Q_ρ/Q_u is the ratio between the density and turbulent kinetic energy dissipation. Starting with isotropic conditions brings the important property that the initial density-velocity covariances are all zero, which reduces the addition in non-neutral stratification to the density spectrum alone.

Following [1], the dimensionless eddy break-up time scale under neutral stratification can be written in terms of the hypergeometric function

$$\tau_{M94} = \frac{\Gamma}{\alpha}k^{-2/3}\left[{}_2F_1\left(\frac{1}{3},\frac{17}{6};\frac{4}{3};-k^{-2}\right)\right]^{-1/2}, \tag{18}$$

where Γ is the anisotropy parameter. The presence of the oscillation time scale introduced by the Brunt-Väisälä frequency suggests a new time scale, τ, here assumed to be of the form

$$\frac{1}{\tau} = \frac{1}{\tau_{M94}} + cN \longrightarrow \tau = \frac{\tau_{M94}}{1+cN\tau_{M94}}\,. \tag{19}$$

The advantage of this assumption is that the neutral time scale is kept exactly as in [1] and the stability dependence comes from an independent parallel coupling of τ with N by the constant c. Besides the scaling quantities U_s and L and the initial spectral tensor parameters Q_u and Q_ρ, two other parameters are therefore needed to complete the model by determining the break-up time scale, namely Γ and c. By assuming that U_s is equal to the streamwise velocity standard deviation σ_u, and according to the observations done in Ryningsnäs, some of these parameters can be assumed to be constant (Γ and c) or function of the Richardson number (Q_ρ/Q_u and z/L), as discussed in [6].

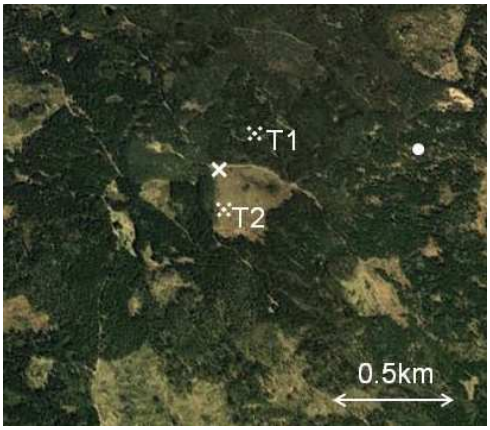

Figure 1. Landscape of the Ryningsnäs site.

3. Experimental setup

The experiment took close to the inland mansion of Ryningsnäs in Sweden, located 30 km inland from the Swedish south-eastern coast. A complete description of the site and the equipment has been reported by Arnqvist *et al.* [9] and here only some brief details are recalled. A 138 m tall meteorological tower was located in the northwestern corner of a 200 m by 250 m large clearing surrounded by a forested area consisting of predominantly Scots Pine trees (with a mean canopy height of $h_c = 20$ m). Two wind turbines, labeled T1 and T2 in figure 1, are located approximately 200 m (corresponding to 2.2 rotor diameters) from the tower in the southern and north-eastern directions, respectively. The hub height is $z_{\mathrm{hub,T1}} = 100$ m and $z_{\mathrm{hub,T2}} = 80$ m, for the turbine T1 and T2, respectively.

The experiment ran between November 2010 and February 2012, yielding a total of 10560 hours of available measurements. 6 tri-axial Metek sonic anemometers were placed at $z =$ 40, 59, 80, 98, 120, 137.7 m complemented by additional Risø PT-100 temperature sensors at $z = 40$, 98, 120, 137.7 m. The data were first sorted into 30-min blocks and, for each 30-min time series, statistics were computed. At each measurement height the velocity components were also rotated to a Cartesian reference frame xyz where the average lateral velocity, V, was zero. The data were sorted according to the velocity at $z = 100$ m (in bins of 1 m/s) and to the ratio h_c/L_o, where L_o is the Obukhov length, evaluated by means of the conventional definition

$$L_o = -\frac{u_*^3 \Theta_0}{\kappa g \left\langle w'\theta' \right\rangle}\,, \tag{20}$$

where $\kappa = 0.4$ is the von Kármán constant, $\langle w'\theta' \rangle$ is the vertical temperature flux determined from the sonic anemometer at the lowest height, Θ_0 is the reference temperature taken from the temperature sensor at the lowest height, and u_* is the friction velocity that is consistently evaluated at the lowest height ($z = 40$ m), by $u_* = \left[\langle w'u' \rangle^2 + \langle v'w' \rangle^2\right]^{1/4}$.

The western sector (with direction within $[240°, 280°]$) was defined as the sector where the influence from the two turbines and the clearing was minimal (see [9] for a discussion regarding the nearby clearing effects). Luckily, the western sector was also coincident with the most probable mean wind direction as well as being the direction with the longest upwind forest cover.

4. Results

The model parameters have been calibrated against single-point spectra measured at Ryningsnäs in the velocity bin where $U(z = 100 \text{ m}) \approx 8 \text{ ms}^{-1}$. Figure 2 shows a comparison between the measured and modelled pre-multiplied spectra. Obviously the agreement here is a result of the fitting method (which determines the parameters L, Q_u, Q_ρ, Γ and c by maximising the agreement between the measured and modelled pre-multiplied single-point velocity and temperature spectra at some frequencies), although it is worth to notice that the $u\theta$ spectrum was not used in the parameters determination, which can be considered here as an indicator of the quality of the model. The single-point temperature spectra have not been shown as the measured spectra for near-neutral to moderately stable conditions shows limited quality with large high frequency scatter. This is a known problem of sonic anemometers and does not affect the co-variances [10]. Due to the high frequency scatter causing upward tails of the spectra and the subsequent problem with model comparison the temperature spectra have not been considered in the present analysis.

At this point, it is worth computing the integral of the spectra providing the measured velocity and temperature covariances, shown in figure 3. It is visible that the model is able to compute the velocity variances and the shear stress $\langle u'w' \rangle$ as well as the heat fluxes $\langle u'\theta' \rangle$ and $\langle w'\theta' \rangle$. All these integral quantities appear to be well estimated, underlining the fact that the present model complements [1, 2, 4]. The only information going in to the model is the background stratification and shear as well as horizontal velocity variance. It seems thus that the mean distortion by temperature and velocity gradients is enough to reproduce the same distribution of energy between different Reynold stress components and heat fluxes that is observed in nature.

Both single-point spectra and associated integrals are however a direct result of the fitting of the spectra and their agreement with the measurements is expected. The fitting process was performed by using only single-point data with no information about two-point spectra. Therefore a comparison of the model prediction with two-point spectra represents a way to validate the proposed model. Figures 4 and 5 show two-point data that assess how well the model performs. Figure 4 shows the covariance between two different heights for the uu, vv, ww cross spectra in three different stability conditions (from nearly neutral to stable). The covariances are here normalised with the product of the standard deviations of the relative velocity components at the heights z_1 and z_2, and plotted against the height difference $\Delta z = |z_2 - z_1|$ normalised by the average wind speed $\overline{U} = [U(z_1) + U(z_2)]/2$. The advantage of this normalisation is discussed in [11] where it is demonstrated that the data collapse well. As visible in the figure, the modelled covariances have the same qualitative behaviour of the measured data, although with a slight overestimation of the covariances (especially in uu). The stability trend is correctly predicted for all the velocity components.

Figure 5 shows the comparison between the phase of the cross-spectra between the two different heights (for a frequency of 0.01 Hz) against the variable $\Delta z/\overline{U}$ where a monotonic trend is visible (except for ww that is scattered around a zero-phase shift). Here the model is able to qualitatively follow the data trend but the phase shift is slightly underestimated. No significant stability trend can be discerned in both measurements and modelled phases. Noteworthy, the phases follow the inequality $\phi_w < \phi_u < \phi_v$ proposed by [12] for neutral stratification.

5. Conclusions

In the present paper a new model to estimate the velocity and temperature spectral tensor of the atmospheric boundary layer is proposed. The model is based on an analytical solution of the stratified RDT equations for a homogeneous turbulent flow subjected to homogeneous shear and stable stratification. This approach allows to determine the time-wise evolution of the Fourier transform of the velocity and density fluctuations starting from an arbitrary initial

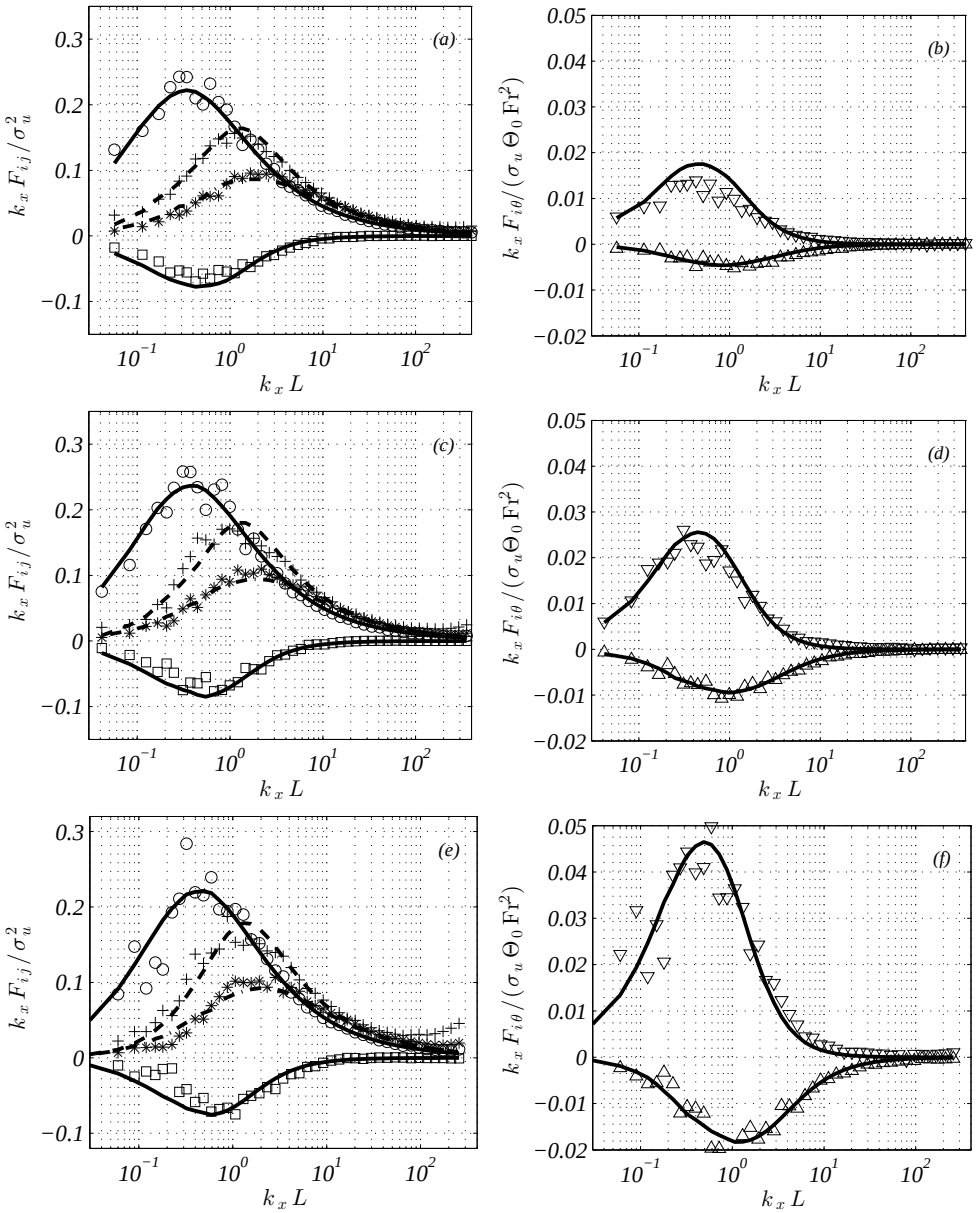

Figure 2. Comparison of the pre-multiplied spectra at $z \approx 138$ m and $U(z = 100\ \mathrm{m}) \approx 8\ \mathrm{ms}^{-1}$ for $(a - b)$ Neutral conditions (Ri ≈ 0.07), $(c - d)$ Near-Neutral Stable conditions (Ri ≈ 0.10) and $(e - f)$ Stable conditions (Ri ≈ 0.14). Experimental data: $(\circ)$ F_{uu}, $(+)$ F_{vv}, $(*)$ F_{ww}, $(\square)$ F_{uw}, $(\bigtriangledown)$ $F_{u\theta}$, $(\bigtriangleup)$ $F_{w\theta}$. Model: (*solid line*) F_{uu}, F_{uw}, $F_{u\theta}$, $F_{w\theta}$. (*dashed line*) F_{vv}. (*dash-dotted line*) F_{ww}.

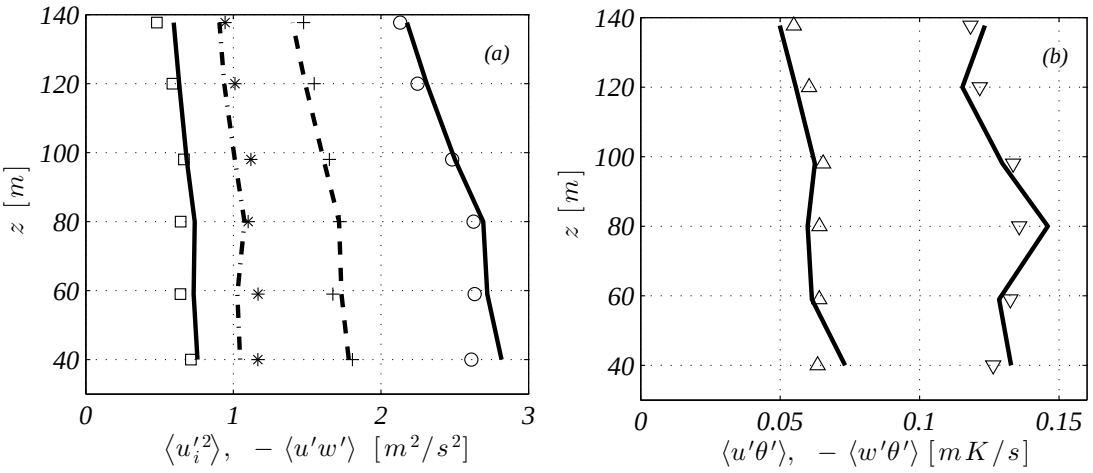

Figure 3. Comparison of the integral of the single-point spectra when $U(z = 100\text{ m}) \approx 8\text{ ms}^{-1}$ for Near-Neutral Stable conditions ($\text{Ri} \approx 0.10$) for zero separation distance. Experimental data: ($\circ$) $\langle u'^2 \rangle$, ($+$) $\langle v'^2 \rangle$, ($*$) $\langle w'^2 \rangle$, ($\square$) $-\langle u'w' \rangle$, ($\triangledown$) $\langle u'\theta' \rangle$, ($\triangle$) $-\langle w'\theta' \rangle$. Model: (*solid line*) $\langle u'^2 \rangle$, $-\langle u'w' \rangle$, $\langle u'\theta' \rangle$, $-\langle w'\theta' \rangle$. (*dashed line*) $\langle v'^2 \rangle$. (*dash-dotted line*) $\langle w'^2 \rangle$.

state, as long as the rapid-distortion closure is valid. By following the same approach of Mann [1], the equilibrium state of the time-dependent spectral tensor is determined by introducing a wavenumber-dependent time scale.

The model is based upon a number of scaling quantities and parameters. These have all been determined by optimising the comparison between model outputs and measurements over a forested area [2, 9]. According to our observations, the proposed model is able to determine reasonably well the single-point velocity spectra and the single-point velocity and temperature cross-spectra (including $F_{u\theta}$, which was purposefully kept out of the optimisation approach) for different Richardson numbers. Although the model is a function of only one initial velocity scale and one initial temperature scale it predicts the same distribution of energy between all the different covariances as is observed in the measurements. This suggests that in turbulent flows at the height span and velocity range that is interesting to wind energy the rapid distortion equations provide a valid approximation to the flow in a statistical sense. When evaluated against vertically separated two-point spectra, the model showed qualitative agreement with the available data both in terms of decay with separation distance and the tendency of decreasing correlation with increasing stratification.

References

[1] Mann J 1994 *J. Fluid Mech.* **273** 141–168
[2] Chougule A, Mann J, Segalini A and Dellwik E 2014 *Wind Energy* **18** 469–481
[3] Hanazaki H and Hunt J C R 2004 *J. Fluid Mech.* **507** 1–42
[4] Chougule A 2013 *Influence of atmospheric stability on the spatial structure of turbulence* Ph.D. thesis DTU Wind Energy
[5] Townsend A A 1976 *The structure of turbulent shear flow* (Cambridge University press)
[6] Segalini A and Arnqvist J 2015 *J. Fluid Mech.* **submitted**
[7] Kaimal J C, Wyngaard J C, Izumi Y and Coté O R 1972 *Q. J. Roy. Meteor. Soc.* **98** 536–589
[8] Goedecke G H, Ostashev V E, Wilson K D and Auvermann H J 2004 *Bound.-Lay. Meteor.* **112** 33–56
[9] Arnqvist J, Segalini A, Dellwik E and Bergström H 2015 *Bound.-Lay. Meteor.* DOI 10.1007/s10546–015–0016–x
[10] Nielsen M and Larsen S E 2002 *The influence of pulse-firing delays on sonic anemometer response characteristics* (American Meteorological Society) pp 139–142

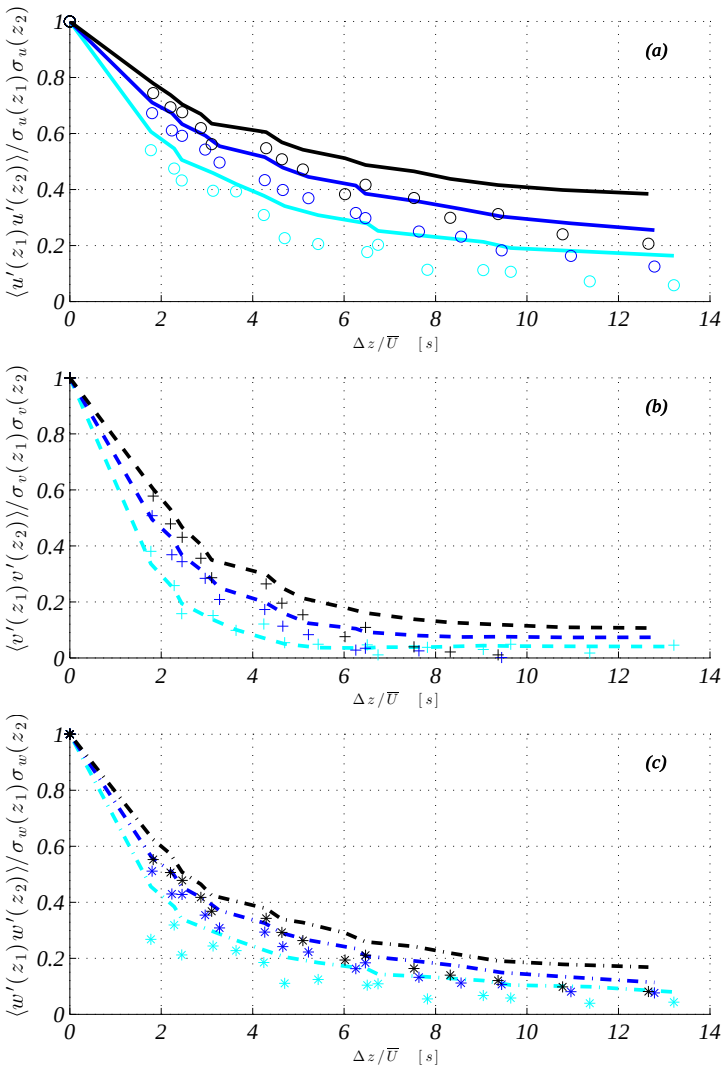

Figure 4. Comparison of the integral of the two-point cross-spectra when $U(z = 100\text{ m}) \approx 8\text{ ms}^{-1}$ for different stability conditions (*black* Ri ≈ 0.07, *blue* Ri ≈ 0.10 and *cyan* Ri ≈ 0.14) between different points at heights z_1 and z_2 between the u-component (a), v-component (b) and w-component (c). Experimental data: $(\circ)$ $\langle u'(z_1)u'(z_2)\rangle$, $(+)$ $\langle v'(z_1)v'(z_2)\rangle$, $(*)$ $\langle w'(z_1)w'(z_2)\rangle$. Model prediction: (*solid line*) $\langle u'^2\rangle$, (*dashed line*) $\langle v'^2\rangle$, (*dash-dotted line*) $\langle w'^2\rangle$.

[11] Bergström H, Alfredsson P, Arnqvist J, Carlén I, Dellwik E, Fransson J, Ganander H, Mohr M, Segalini A and Söderberg S 2013 Wind power in forests: wind and effects on loads Tech. rep. Elforsk Rapport, 13:09
[12] Chougule A, Mann J, Kelly M, Sun J, Lenschow D H and Patton E G 2012 *J. of Turbulence* **13** 1–13

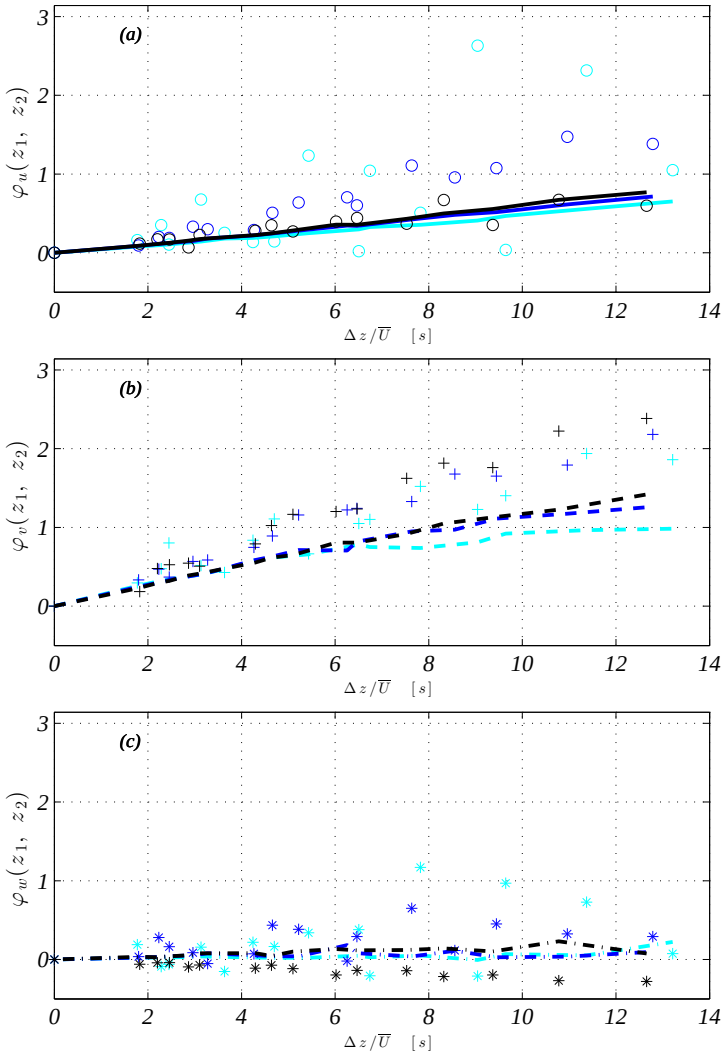

Figure 5. Comparison of the spectral phase when $U(z = 100\text{ m}) \approx 8\text{ ms}^{-1}$ and $f = 0.01$ Hz for different stability conditions (*black* Ri ≈ 0.07, *blue* Ri ≈ 0.10 and *cyan* Ri ≈ 0.14) between different points at heights z_1 and z_2 between the u-component (a), v-component (b) and w-component (c). Experimental data: $(\circ)$ $\varphi_u(z_1, z_2)$, $(+)$ $\varphi_v(z_1, z_2)$, $(*)$ $\varphi_w(z_1, z_2)$. Model prediction: (*solid line*) $\langle u'^2 \rangle$, (*dashed line*) $\langle v'^2 \rangle$, (*dash-dotted line*) $\langle w'^2 \rangle$.